Chapter 4
Results and discussion

4. Results and discussion

4.1 Electrochemical oxidation of DCF

Electrochemical oxidation of DCF was carried out in RO concentrate which was chloride rich (1.6 g/L, refer Table 4). Therefore, the main oxidizing species responsible for degradation would be reactive chlorine species i.e. HOCl, Cl_2, ^{-}OCl and hydroxyl radicals ($^{\bullet}OH$) (Martínez-Sánchez et al., 2022; Szpyrkowicz et al., 2000, 2007). The contribution of hydroxyl radicals was examined using nitrobenzene as a probe. No significant change was observed in DCF degradation, which means that the contribution of reactive chlorine species was much higher than the contribution of hydroxyl radicals. Moreover, the anode selected in this study - DSA type Ti/Ru-Sn-Sb-O_x MMO- was proven to be active and efficient for in situ electro-generation of RCS species from chlorides (Cruz-Díaz et al., 2018; Y. Feng et al., 2016; García-Espinoza & Nacheva, 2019; Y. J. Liu et al., 2019). The prevalence of various reactive chlorine species is pH-dependent. RCS arise as HOCl (hypochlorous acid) and/or OCl^{-}(hypochlorous anions) at near-neutral pH, between 5.5 and 7.5. The pH of ROC used in this study ranges from 6.9 to 7.5, which means HOCl and OCl^{-} were predominant species in the degradation of DCF and its intermediate products(Y. Feng et al., 2016; H. Wang et al., 2019). DCF degradation mechanism can be described as follows: Ti/Ru-Sn-Sb-O_x anode used the electricity supplied in the solution to convert chloride in ROC to chlorine gas (Eq. 2). The chlorine gas reacts with water and HOCl/ClO^{-} are formed at near neutral pH. Giannakopoulos et al., 2022 and Y. Yang et al., 2022 indicated that electro-generated dissolved chlorine is unnoticed yet dominant oxidant for DCF removal. Giannakopoulos et al., 2022 reported the EO of DCF using Pt-SnO_2/Ti anode and the results reported were consistent with our results. These reactive chlorine species are responsible for DCF degradation in ROC at near neutral pH. HOCl and OCl^{-} production in an undivided cell can be described by reactions 2, 3, and 4:

$$2Cl^- \rightarrow Cl_2 + 2e^- \text{ [~1.36 V vs SHE, (Luna-Trujillo et al., 2020)]} \quad (2)$$

$$Cl_2 + H_2O \rightarrow HOCl + H^+ + Cl^- \quad (3)$$

$$HOCl \leftrightarrow ClO^- + H^+ \quad (4)$$

Nonetheless, no other reactive chlorine species (i.e. ClO_3^-, ClO_4^-) were detected in detectable levels. Also, there are no chances of chlorate (ClO_3^-) and/or perchlorate (ClO_4^-) generation because MMO involved in this study does not have high anodic potential. This is one of the advantages of using MMO over non-active anodes i.e. BDD, PbO_2 while working in a chloride-rich matrix like ROC (Aquino et al., 2012; Barazesh et al., 2016; Y. Feng et al., 2016). To prove the hypothesis that RCS production in large amounts in chloride rich ROC is because of reactions 2, 3, and 4, the concentration of RCS over the time at various current densities is shown in Figure 7.

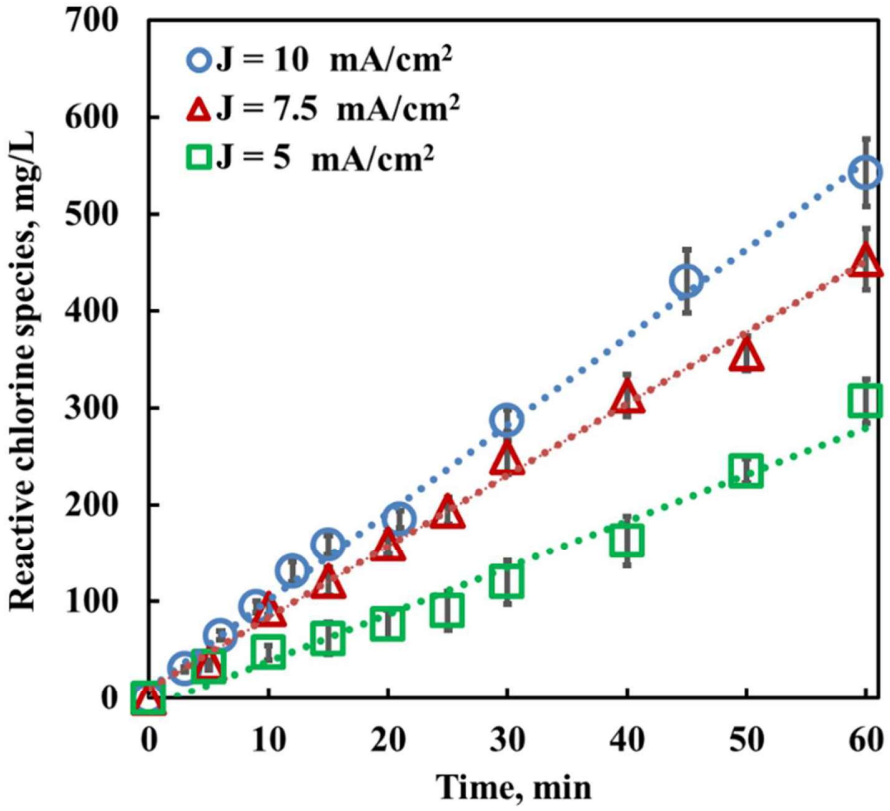

Figure 7: Formation of reactive chlorine species along the time

4.2 Effect of quenching agents on EO of DCF

It was necessary to determine the concentration of reactive chlorine species to determine the dose of the quenching agent. The concentration of reactive chlorine species along the time is shown in Figure 7. The effect of various quenching agents is shown in Figure 8.

Immediate analysis without quenching: Time course profiles resulting from electrochemical oxidation of DCF in RO concentrate matrix are illustrated in Figure 8 (refer Appendix D for corresponding HPLC chromatograms). Figure 8a shows the scenario of immediate analysis. More than 90% of the initial DCF was removed in 25 minutes. Other than DCF (retention time: 9.6 min), two main intermediates can be observed, $IP_{8.5}$ (retention time: 8.5 min) and $IP_{9.1}$ (retention time: 9.1 min) in HPLC chromatograms (Figure 9). DCF was rapidly degraded and intermediates are rapidly formed in 25 minutes. After 25 minutes, removal was increased by 2% only, from 94% to 96% in the last 35 minutes. Maximum intermediates are observed at the 40^{th} minute, after this, intermediates also start decreasing.

Quenching with Sodium sulfite: Sodium sulfite is a widely used reducing agent for quenching reactive species. (Keen et al., 2013; Kristiana et al., 2014; M. Yang & Zhang, 2016). It is added in excess to ensure complete quenching (Kristiana et al., 2014; Luongo et al., 2021). As per Figure 7, a maximum of 453 mg/L reactive species are electrochemically generated while applying 7.5 mA/cm^2 current density, therefore 5 mL samples are withdrawn at different time points and quenched with 0.25 mL of 15 g/L sodium sulfite, which gives 476 mg/L sulfite in samples. It can be observed from Figure 8b, that concentration of DCF was decreased from actual concentration when samples are quenched with sulfite. The concentration of DCF and intermediate products in quenched samples are depicted through dotted lines in Figure 9. Surprisingly, intermediates have vanished when sulfite was added (see Figure 9b). The reason behind this is the ability of sulfite to reduce halogenated compounds and azo-aromatic compounds (Diana et al., 2019; How et al., 2017). Intermediate products are possibly reduced by sulfite and that is why they are not detected in the sample. Here, the concentration of sulfite is much higher than DCF and intermediate products concentration, this could also be the reason. This false negative determination of intermediate products can mislead the investigation and researchers may draw the wrong conclusions. Kristiana et al., 2014 and Yang & Zhang, 2016 also reported in their studies

that sulfite cannot be used while studying the halogenated organic compounds. Kristiana et al., 2014 showed that sodium arsenite is the alternative to sodium sulfite while working with halogenated organic products.

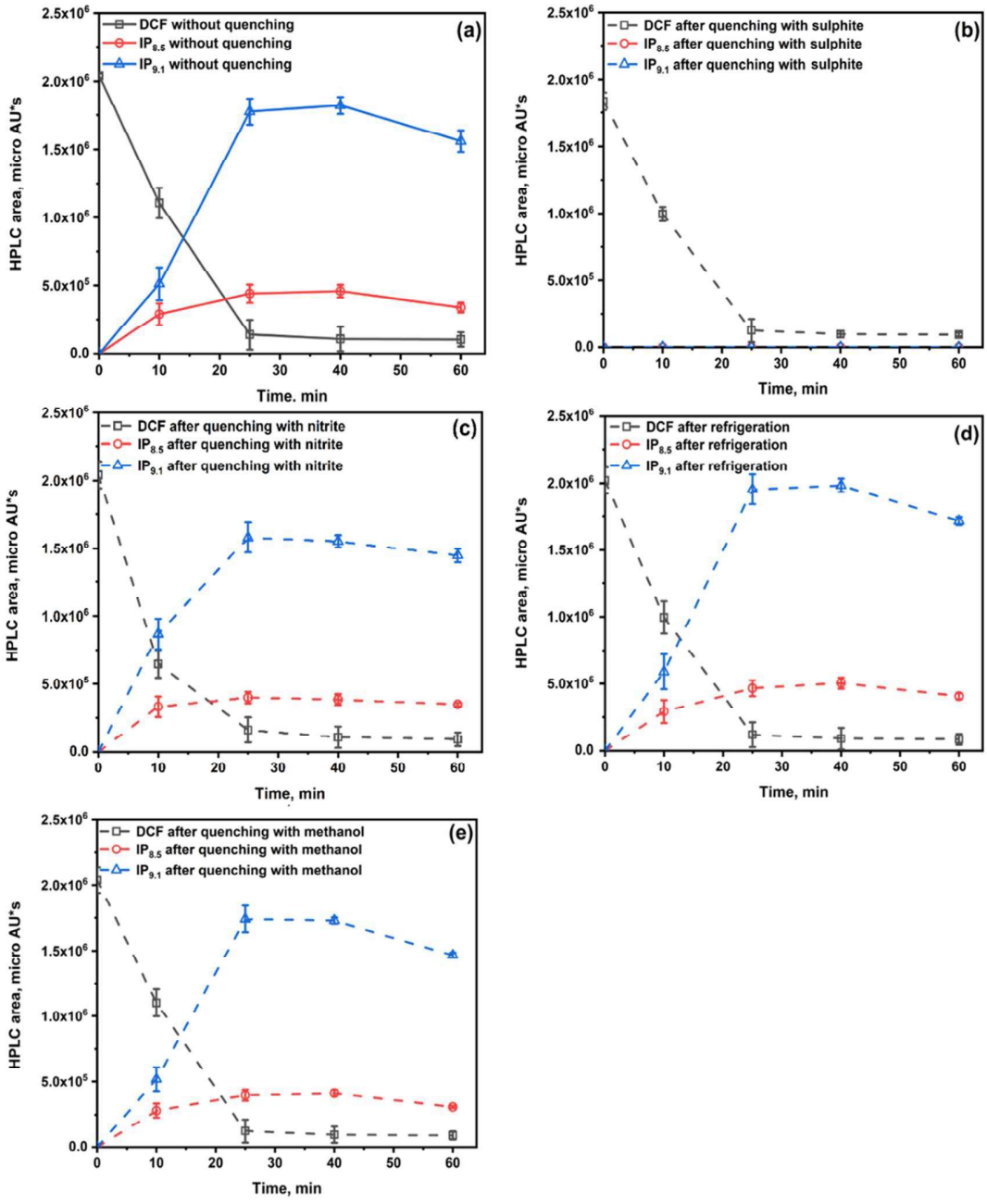

Figure 8: Area covered under chromatogram along the time (a) for immediate analysis without quenching, (b) analysis after quenching with sodium sulfite, (c) analysis after quenching with sodium nitrite, (d) analysis after 24 h refrigeration at 4^0C, (e) analysis after quenching with methanol

Quenching with sodium nitrite: In general, sodium nitrite is used as a quenching agent when a sample is subjected to TOC analysis (Shukla et al., 2010; F. Zhang et al., 2020). Similar to sodium sulfite, sodium nitrite is a reducing agent and is added in excess to ensure quenching of all reactive species. As per Figure 7, a maximum of 453 mg/L reactive species are electrochemically generated, therefore, 5 mL samples are withdrawn at different time points and quenched with 0.25 mL of 15 g/L sodium nitrite, which contains 500 mg/L nitrite. It can be observed from Figure 8c that after quenching with nitrite, the concentration of DCF is decreased and the concentration of intermediate products is increased (dotted line) in comparison with actual concentration (solid line) for T=10 min sample. It has been reported by Eiserich et al., 1996, that reaction between nitrite ions and OCl^- ions at near neutral pH leads to formation of $Cl^\bullet$, $^\bullet NO$, and $^\bullet NO_2$. Such radicals, for example, $Cl^\bullet$ is shown to chlorinate aromatic compounds namely tyrosin containing hydroxyl and carboxylic groups. Thus, in our case, in the samples quenched with nitrite ions, the chlorination of DCF may continue resulting in reduction in peak area of DCF with concomitant increase in the peaks of intermediates. Afterward, intermediate products kept decreasing and DCF is more or less similar to actual data because there is no enough DCF to further react with $Cl^\bullet$, $^\bullet NO$, and $^\bullet NO_2$. Though this is better than sulfite quenching, it is not the same as fresh samples. Figure 9c shows the overlay chromatograms where the blue line indicates sample quenched with nitrite and the black line depicts fresh samples without quenching.

Refrigeration for preservation: Refrigeration is widely used technique for preserving the samples (García-Fernández & Roy Editor, 2020; Salazar et al., 2018). Samples were preserved in the fridge at 4 ^{0}C for 24 h and then preserved samples were analyzed in HPLC. Unlike chemical quenching, reactive species become inactive because of temperature drop, and DCF as well as intermediate products concentration remain the same as fresh samples. It is observed from Figure 8d, that the HPLC area and trend remain mostly the same. It can be observed from Figure 9d that the shape of HPLC peaks is different but the area does not change significantly. It is advisable to use refrigeration in place of chemical quenching using sulfite or nitrite.

Quenching with Methanol: In recent times, methanol is used to quench reactive species because methanol is readily oxidized in comparison with other organic compounds to be analyzed (Ahn & Yun, 2019; Shukla et al., 2010). The reaction rate constant for methanol degradation is many-fold higher than other target organic compounds. Moreover, it is not a reducing agent and

does not interfere with the sample matrix or intermediates. To determine the most suitable ratio for methanol volume to sample volume, four different ratios were tested- 20:80, 30:70, 40:60, and 50:50, for T = 10 min sample as it contains DCF and both intermediate products. Area obtained from HPLC were multiplied by 1.25, 1.428, 1.667 and 2 for ratios 20:80, 30:70, 40:60, and 50:50 respectively (refer to Appendix A). Results show that 50:50 is the most suitable ratio for quenching purposes. As per Figure 8e, samples quenched with methanol match perfectly with the actual trend. Figure 9e compares the chromatogram of sample without quenching – (diluted 1:1 with distilled water) with a chromatogram obtained after quenching with methanol (sample: methanol = 1:1). It can be observed that both the chromatograms very closely match with each other.

Quenching with NaOH to Alkaline pH (pH>10): As per basic chlorination chemistry, hypochlorous acid (HOCl) is completely converted to a hypochlorite ion ($^{-}$OCl) above pH 10. That is why, this experiment was carried out, to check whether HOCl conversion helps or not. It was observed that along with HOCl, DCF and its intermediate products were also precipitated and no peaks were found in HPLC (refer Appendix B). It is not advisable to use this technique. Correlation test and Paired t-test were carried out for various data groups to statistically support the results and conclusion of Quenching experiments (refer Appendix E). Among various agents/techniques, methanol quenching and refrigeration showed better correlation ($R^2 \geq 0.99$) and nitrite showed reasonable correlation ($R^2 = 0.94$). However, p values obtained using paired t-test were 0.005, 0.1, and 0.3 for methanol quenching, 24 h refrigeration, and nitrite quenching respectively. These values indicate that the results obtained using methanol as a quenching agent matches with those obtained by immediate analyses (without quenching) with 99.5% confidence level. Thus, methanol is the most suitable quenching agent in the present study.

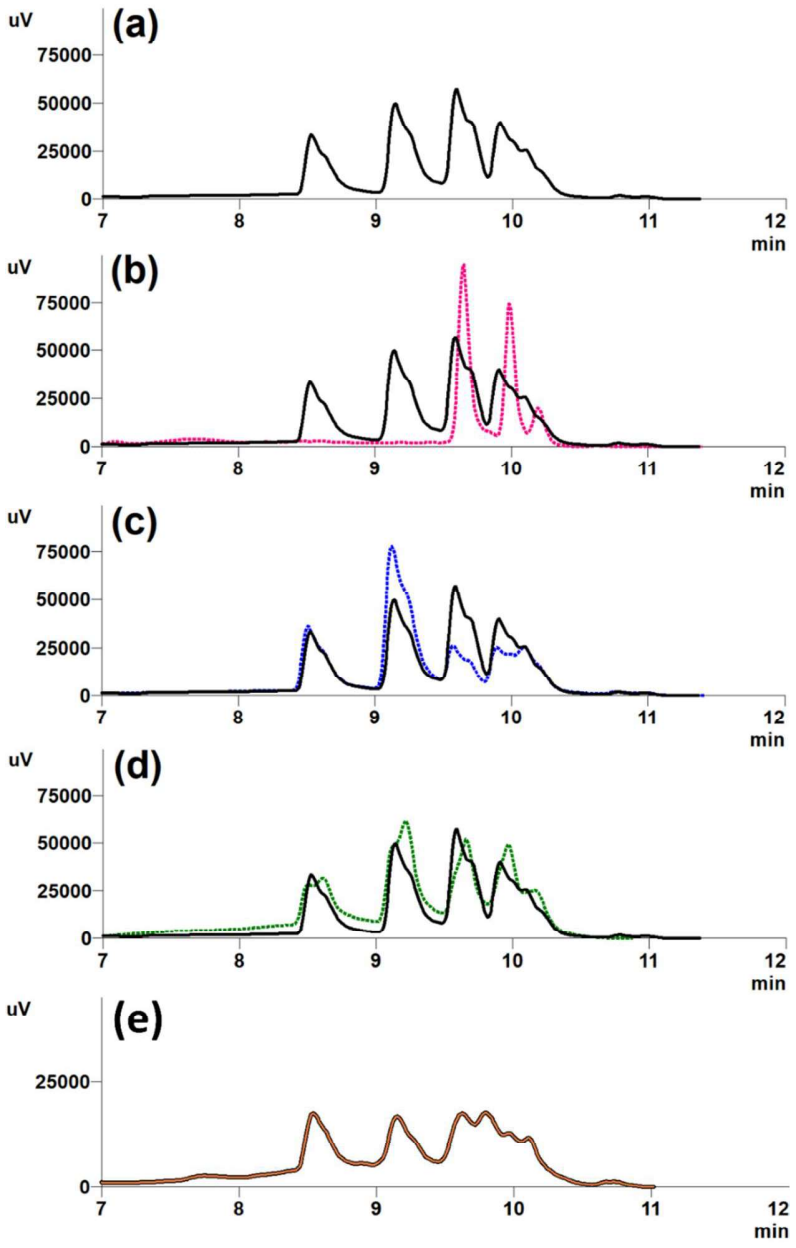

Figure 9: HPLC chromatograms for 10 min reaction time, dotted line represents result after quenching and solid black line represents immediate result without quenching (a) solid black line - for immediate analysis without quenching, (b) dotted pink line - analysis after quenching with sodium sulfite, (c) dotted blue line - analysis after quenching with sodium nitrite, (d) dotted green line - analysis after 24 h refrigeration at 4 ^{0}C, (e) thin orange line - analysis after quenching with methanol (sample: methanol = 1:1) overlaid on solid black line – 1:1 diluted sample with distilled water

4.3 Effect of the applied current density and reaction kinetics

Various current densities of values 5, 7.5, and 10 mA/cm^2 were applied to examine the electrochemical oxidation of DCF and its intermediate products in ROC. As shown in Figure 10, increase in current density has resulted in faster and complete removal of DCF and its intermediate products. For lower current density J=5 mA/cm^2, DCF was not completely removed even after 120 minutes, and intermediate products were also there. Increasing current density by 2.5 mA/cm^2 induced faster removal and 98% of DCF and its intermediate products were removed after 120 minutes when applied current density was 7.5 mA/cm^2. Further increase in current density by 2.5 mA/cm^2 showed rapid removal for DCF and especially for intermediate products. At J = 10 mA/cm^{2}applied density, 99.99% removal was achieved after 120 minutes for both DCF and intermediate products. The reason behind this faster removal with increase in current density must be the increasing rate of RCS generation (Giannakopoulos et al., 2022; Y. J. Liu et al., 2019; Sierra-Rosales et al., 2018). It can be observed by Figure 10 that DCF degradation is quick (in first five minutes), but after the 5th minute time point, for all cases, degradation rate dropped drastically (for 5 min to 120 min). The possible reason for this trend can be explained as follows: HOCl usually causes small changes in the DCF which leads to accumulation of further chlorinated or oxidized DCF. HOCl reactivity is assumed to be higher for DCF in comparison with its reactivity for chlorinated intermediate products (Barazesh et al., 2016; Deborde & von Gunten, 2008). In addition to this, electrophilic substitution and attacks of HOCl on DCF is normally quick and significant. However, after exhaustion of the substitutable sites, oxidation and addition reactions are ordinarily sluggish (Deborde & von Gunten, 2008).

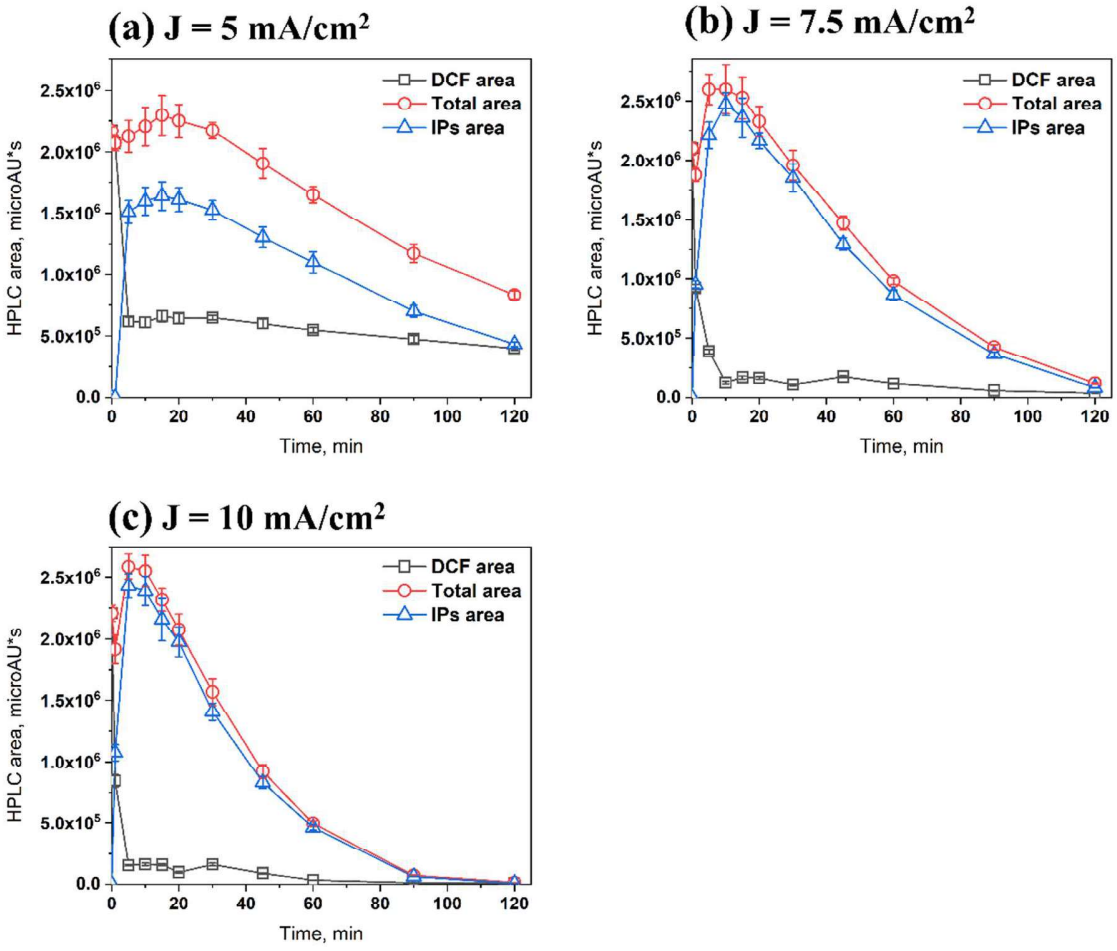

Figure 10: Time course profiles for EO of DCF in ROC, $[DCF]_0$ = 10 ppm, anode: Ti/Ru-Sn-Sb-O_x, cathode: steel, and varying current densities (a) J=5 mA/cm^2, (b) J=7.5 mA/cm^2, and (c) J=10 mA/cm^2.

4.4 Effect of electrolyte composition: sulfate to chloride ratio

Electrolyte composition plays an important role in electrochemical oxidation, particularly in indirect electrochemical oxidation which involves diverse reactive chlorine species and/or reactive oxygen species depending upon the electrolyte. Composition of ROC and other real wastewater matrices is dominated by the presence of two main anions, chloride and sulfate ions. The relative concentration of these salts directly affects the formation of reactive species and ultimately the pollutant degradation (Calzadilla et al., 2021; Murrieta et al., 2020; Q. Xiang et al., 2019). To investigate the effect of the relative concentration of these salts on DCF removal, NaCl

and Na_2SO_4 salts were added in distilled water to achieve the desired ratio of sulfate ions to chloride ions (S:C). To begin with, five matrices were studied; only chloride, S:C = 0.6 (1.1- 0.5), S:C = 1.1, S:C = 1.6 (1.1 + 0.5), and only sulfate. 1.1 was found to be most effective among these five matrices. To fine tune this value, two more ratios were tried, S:C = 0.85 (1.1 – 0.25) and S:C = 1.35 (1.1 + 0.25). These experiments were carried out with 1 L solution at neutral pH and applied current density was 7.5 mA/cm^2 for 120 minutes.

Figure 11 shows the time course profiles for DCF, intermediate products, and total (DCF + intermediate products) area for all seven different matrices. It can be observed that early DCF degradation rate increased with increase in chloride concentration but after a certain point when intermediate products reached their maximum, further degradation turned out to be extremely slow. On the other hand, DCF degradation rate is 0.6 times lesser for only sulfate matrix than only chloride matrix. If we observe the extent of degradation, only chloride or only sulfate matrices are not at all suitable. When moving from S:C = 0 :1 to S:C = 0.6:1, it can be observed that initial degradation was slower but no significant change was there in total area. Moving ahead, in case of S:C = 0.85 :1, total area was removed noticeably and in case of S:C = 1.1 :1, total area removal was maximum. The ratio S:C = 1.1 :1 was found to be the most effective ratio among all. Forging ahead, increase in sulfate from 1.1 to 1.35 did not show any significant change in removal trend but extent of removal was slightly affected, total area removal was a little lesser (3%). Increase from 1.35 to 1.6 negatively affected total area removal and degradation rate. In only sulfate medium, there was no removal in total area and DCF was kept slowly transformed to intermediate products, this matrix showed worst performance among all.

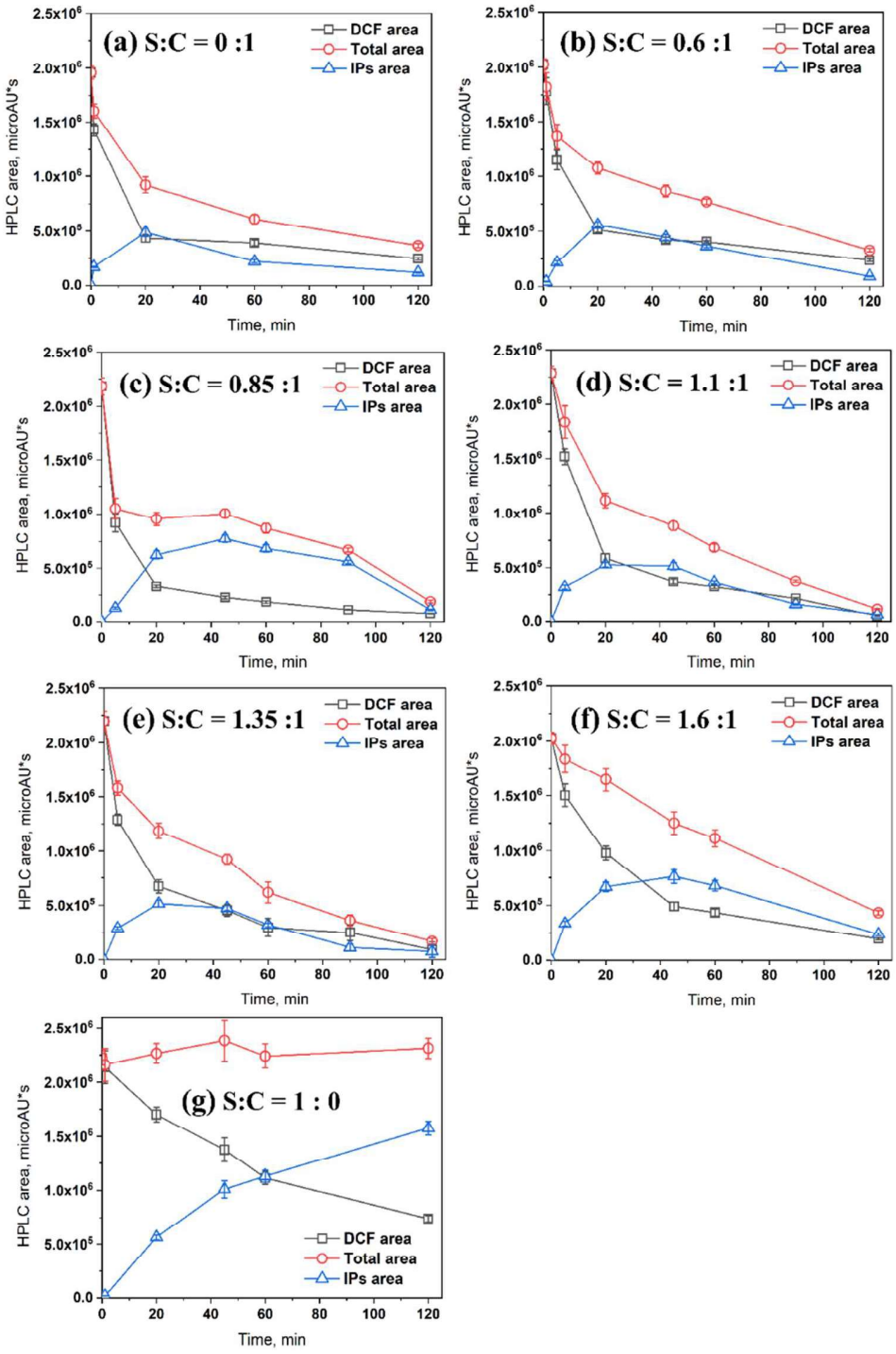

Figure 11: Effect of sulfate to chloride ratio on EO of DCF and its intermediate products, $[DCF]_0$ = 10 mg/L, J = 7.5 mA/cm^2, total salt concentration = 1000 mg/L, anode: Ti/Ru-Sn-Sb-O_x, cathode: steel, (a) [NaCl] = 1000 mg/L and S:C = 0 : 1, (b) [Na_2SO_4]:[NaCl] = 350 : 650 and S:C = 0.6 : 1, (c) [Na_2SO_4]:[NaCl] = 460 : 540 and S:C = 0.85 : 1, (d) [Na_2SO_4]:[NaCl] = 500 : 500 and S:C = 1.1 : 1, (e) [Na_2SO_4]:[NaCl] = 550 : 450 and S:C = 1.35 : 1, (f) [Na_2SO_4]:[NaCl] = 600 : 400 and S:C = 1.6 : 1, (g) [Na_2SO_4] = 1000 mg/L and S:C = 1 : 0.

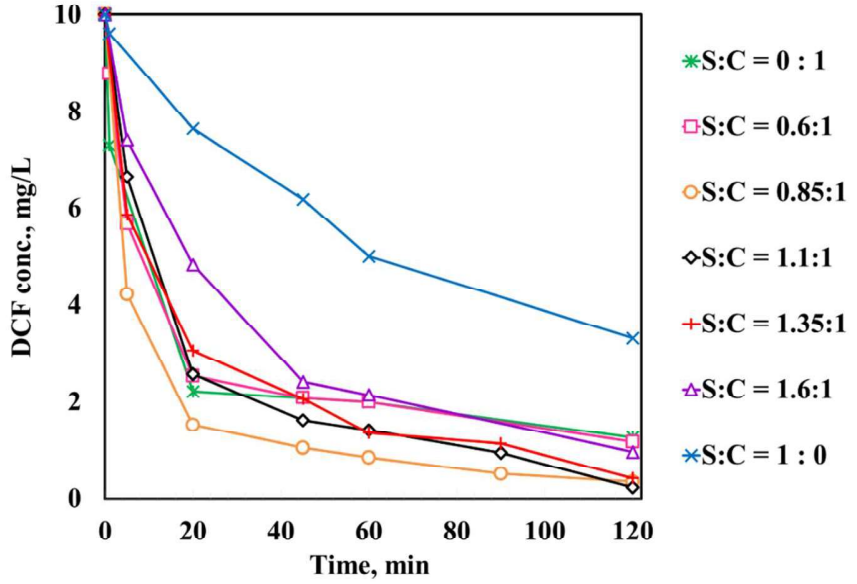

Figure 12: Time course profile for DCF in various S:C composition, J = 7.5 mA/cm^2, Ti/Ru-Sn-Sb-O_x anode, steel cathode, solution volume = 1 L, $[DCF]_0$ = 10 mg/L.

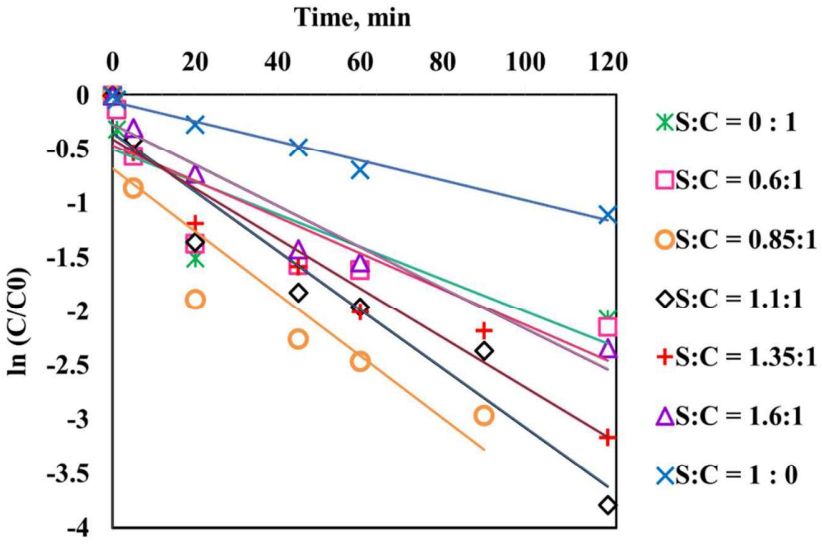

Figure 13: ln(C/C_0) versus time plot for DCF in various S:C composition, J = 7.5 mA/cm^2, Ti/Ru-Sn-Sb-O_x anode, steel cathode, solution volume = 1 L, $[DCF]_0$ = 10 mg/L.

There are two ways of looking at these results, first is from degradation rate point of view, and second is extent of removal point of view which is total HPLC area removal in this case. Figure

13 shows the time course profiles of DCF and Figure 14 shows ln (C/C_0) versus time profiles for all S:C ratios. It can be seen from both the figures that sulfate adversely affects the degradation rate of DCF in comparison with chloride, yet it is not always true. If we carefully observe the trend of DCF removal over 120 minutes, reaction rate constant increases from 0.015 min^{-1} to 0.029 min^{-1} for S:C = 0 to 0.85. For S:C >0.85, reaction rate constant started decreasing to -0.019 min^{-1} for 1.6, and it was dropped to 0.009 min^{-1} for only sulfate matrix. This is clearly shown in Figure 14. Giannakopoulos et al., 2022 reported a first-order reaction rate constant of 0.0394 min^{-1} for $[DCF]_0$=0.5 mg/L, 0.1 M Na_2SO_4 as electrolyte, and current density=16 mA/cm^2, using Pt-SnO_2 coated Ti anode. If we observe the extent of removal, addition of chloride significantly affects the removal (from 1% to 83% for only sulfate to S:C = 1.6 :1 respectively). The extent of removal for all S:C ratios can be assessed from Figure 14. It should be noted that increase in chloride not always helps in total area removal as there is drop from 98% (S:C = 1.1, roughly 48% chloride) to 86% (only chloride, 100% chloride). Hence, it can be concluded that the range 0.85<S:C<1.35 is the suitable range for DCF degradation and overall extent of removal.

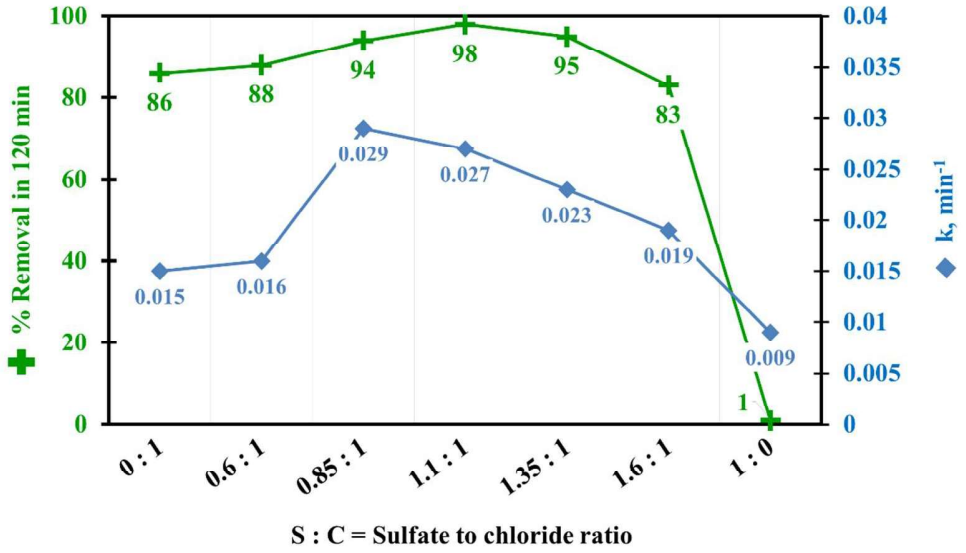

Figure 14: Reaction rate constants for pseudo first order reaction kinetics along with overall (DCF and intermediate products) % removal for various S:C ratios

It is noteworthy that S:C=1.1 gives maximum removal for DCF and intermediate products (98%) in synthetic matrix. To further verify this, required amount of sulfate was added in ROC so

as to keep S:C = 1.1, and this was used as electrolyte and EO was performed at J = 7.5 mA/cm^2. The result was totally in agreement with previous experiment done in synthetic matrix. Total removal reached to 99% after sulfate addition. This improvement can be explained from below mentioned reaction:

$$Cl^{\bullet} + SO_4^{2-} \rightarrow SO_4^{-\bullet} + Cl^- \quad (5)$$

As per Eq. 5, in presence of sulfate ion, $Cl^{\bullet}$ reacts with sulfate and this leads to sulfate radical generation to destruct DCF and its intermediate products (Lan et al., 2017). The composition of electrolyte in terms of sulfate to chloride mass ratio was found to affect the removal of DCF and intermediate products. The maximum removal (~95%) of DCF was obtained in the presence of sulfate to chloride mass ratio ranging from 0.85 to 1.35. It can be observed from Figure 14 that increase in sulfate concentration (sulfate to chloride mass ratio > 1.35) adversely affect the DCF removal. Overall, the increase in chloride concentration, increases rate and extent of DCF removal. However, at the higher concentration of chloride (sulfate to chloride mass ratio <0.85), initially higher degradation rate of DCF (0 to 40 min) is significantly retarded (40 to 120 min). It seems that, increased chlorination due to high concentration of chloride ions, may lead to production of highly chlorinated intermediates which resists further degradation.

4.5 Effect of electrode material on EO of DCF

Three different electrodes – i. Ti/Ru-Sn-Sb-O_x, ii. Ti/Ru-Ir-O_x, and iii. Graphite were used as an anode keeping other reaction parameters same, to evaluate the effect of electrode materials on EO of DCF. It can be seen from the Figure 15a, that initially (within five minutes) degradation rate was faster for Ti/Ru-Sn-Sb-O_x, in comparison with other two electrodes. But as the time progressed, DCF degradation was sluggish in case of Ti/Ru-Sn-Sb-O_x. Similarly, in case of Ti/Ru-Ir-O_x, DCF degradation continued for first ten minutes, then degradation remarkably slowed down. However, in case of Graphite, degradation continued till one hour at slower rate,

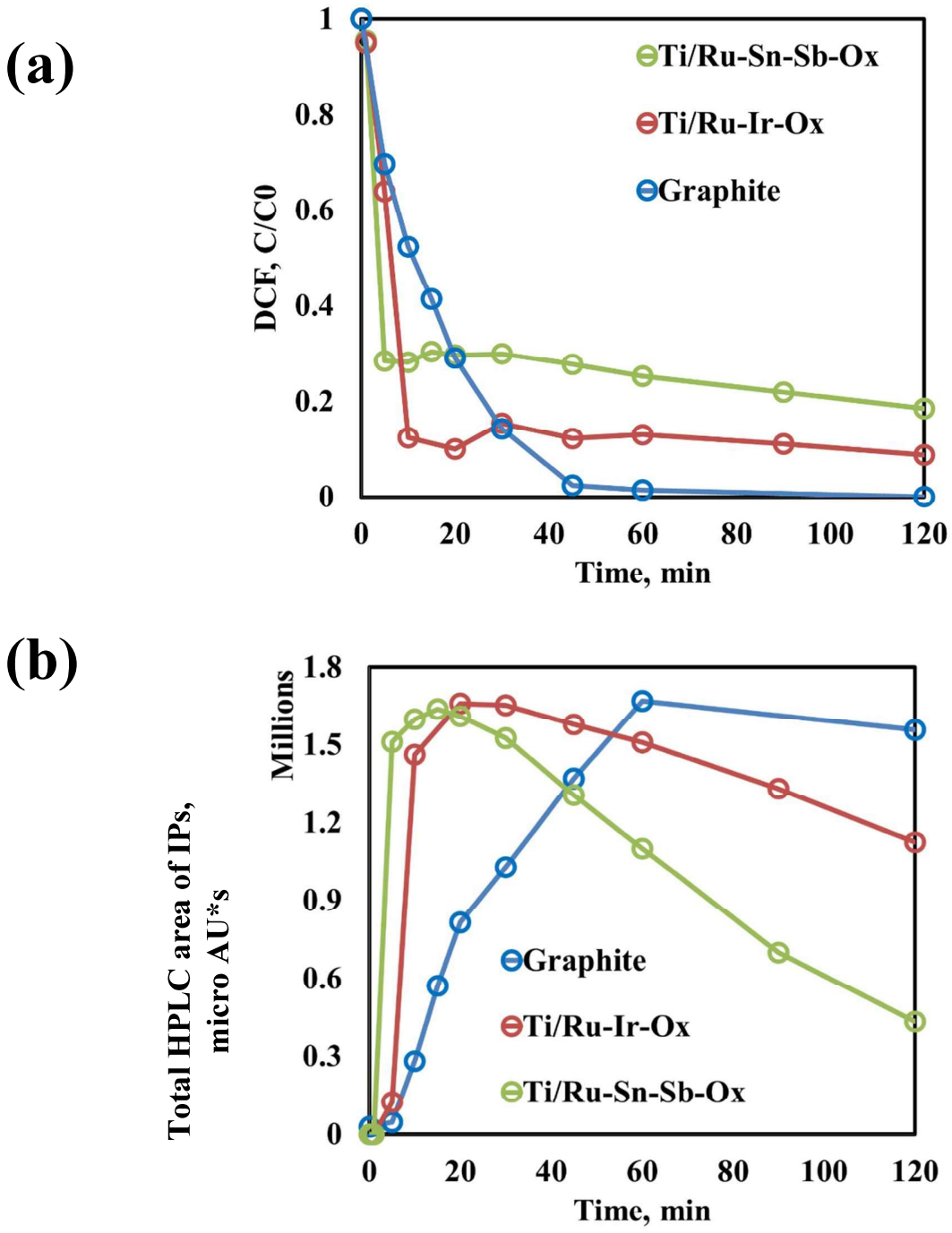

Figure 15: (a) Time course profile for DCF, (b) Total HPLC area of intermediate products, using EO with three different electrodes, matrix = ROC, J = 5 mA/cm^2, steel cathode, solution volume = 1 L, [DCF]$_0$ = 10 mg/L, pH = 7.8

but degradation extent was maximum in this case. DCF was completely removed in two hours but the intermediate products were maximum in case of EO using Graphite (Figure 15b). It can be observed from Figure 15b that intermediates were minimum for EO using Ti/Ru-Sn-Sb-O_x, at the end of two hours. When experiment was carried out at higher densities J = 7.5 and 10 mA/cm^2, graphite plate was started corroding and carbon particles were appearing in solution. Nonetheless, for Ti/Ru-Sn-Sb-O_x and Ti/Ru-Ir-O_x, when higher current densities were applied, degradation rate and extent both were improved. As shown in Figure 10, DCF and its intermediate products were completely removed when applied current density was 7.5 mA/cm^2. Therefore, Ti/Ru-Sn-Sb-O_x was used as an anode for other experiments. The enhanced removal of DCF and its intermediates could be due to electro-catalytic activity of Ru, Sn, and Sb oxides coating (Cruz-Díaz et al., 2018; Martínez-Sánchez et al., 2022).

4.6 Phytotoxicity study

The treatment can be said to be efficient only when high removal efficiency is achieved along with the effluent which is safe to be discharged in environment. To avoid any harm to plants when the treated solution would be applied for irrigation purpose, carrying out phytotoxicity test is necessary. In this study, Mung bean seeds were used for phyto-toxicological analysis of ROC spiked with 10 mg/L DCF, before and after electrochemical oxidation. The results for the study are depicted in Figure 16. Germination % and average radicle length are two crucial parameters in development of plant and also are sensitive towards pollutants (Stupar et al., 2020). Generally, distilled water is taken as control for calculating the phytotoxicity % because most experiments are carried out in synthesized wastewater prepared from distilled water. In this study, distilled water was taken as a check only and ROC was selected as control because ROC was spiked with DCF for EO experiments. Reaction conditions for final sample taken in consideration were: J = 7.5 mA/cm^2, ROC, $[DCF]_0$ = 10 mg/L, Ti/Ru-Sn-Sb-O_x anode steel cathode, pH= 7.5±0.2, and 120 minutes electrolysis time. It can be noted that germination was not significantly affected in comparison with a previously reported study for dye removal using EO which showed 72% after 1780 min of treatment (Mijin et al., 2012). Similarly, for phytotoxicity, initial value was 3% which marginally increased to 9% after 120 min of treatment. It has been reported that any marginal increase in the phytotoxicity after the treatment may not have substantial adverse effect on plant growth (Santos et al., 2020; Vijayakumar et al., 2021). It is important to note that ROC can be used

for irrigation only if the TDS limits and Sodium Adsorption Ratio for the effluent are met. Furthermore, to ensure that there is no uptake of any trace DCF or intermediate products in mung beans, retentate was analysed in HPLC and there was no significant change in HPLC peaks. Also, the experiment was carried out with 2 h of electrochemical oxidation in ROC medium without adding Diclofenac sodium, the results were similar to that of 'Final sample after 30 min' shown in Figure 16. Hence, we can conclude that the phytotoxicity observe here is due to residual HOCl and not the DCF or its intermediates.

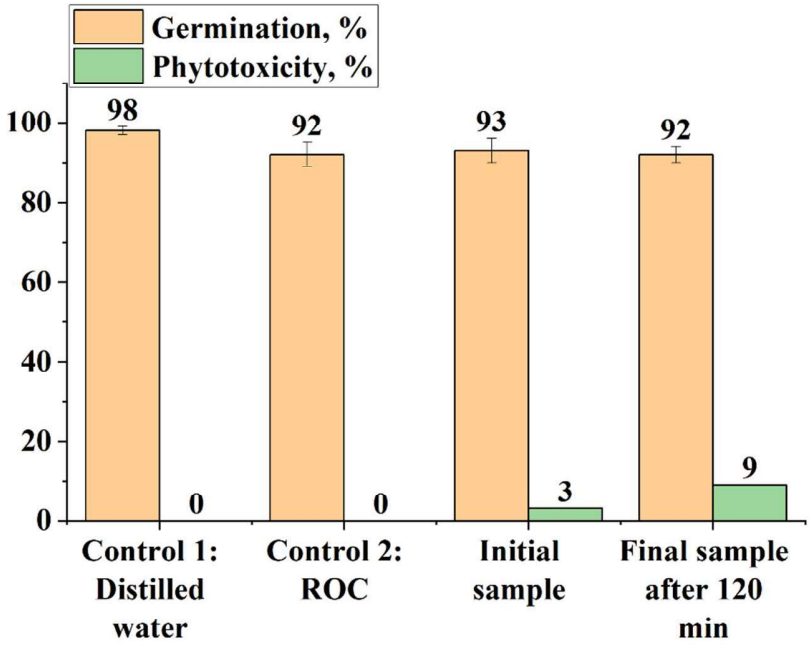

Figure 16: %Germination and %Phytotoxicity for mung seeds in distilled water, ROC, initial sample (ROC spiked with 10 mg/L DCF), and treated sample by EO for 120 minutes

4.7 Comparative study of EC alone, PMS alone, EC/PMS, and Fe_2SO_4/PMS for IBU removal

IBU removal was first observed for five different processes: (a) Electrolysis using iron as an anode (EC alone), (b) PMS alone, (c) Electrochemically activated peroxymonosulfate using iron as anode (EC/PMS process), (d) PMS activation by Fe^{2+} using ferrous sulfate heptahydrate where an equivalent amount of ferrous ($[Fe^{2+}]_0$ = 99.12 mg) was added at the initial point (t=0), and (e) PMS activation by Fe^{2+} where one sixth of an equivalent amount of ferrous ($[Fe^{2+}]_0$ = 16.52

mg) was added in six steps, eventually total Fe^{2+} added in 30 min would be 99.12 mg (16.52 mg Fe^{2+} was added at t =0, 5, 10, 15, 20, 25 min; 6 time points).

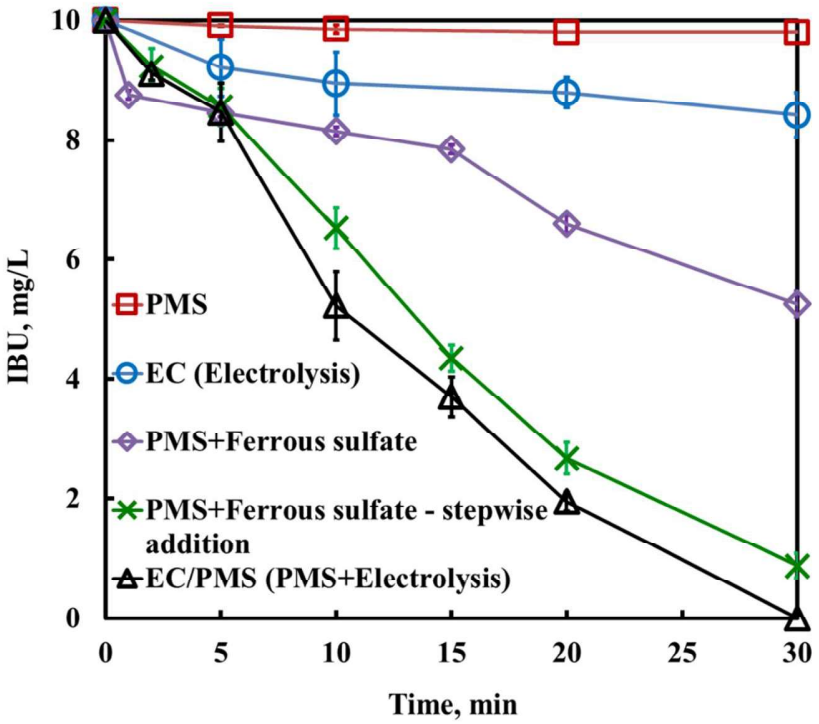

Figure 17: IBU removal in ROC matrix under different systems. Experimental conditions: $[IBU]_0$ = 10 mg/L, $[PMS]_0$ = 500 mg/L, total $[Fe^{2+}]$ = 99.12 mg/L, current density = 2.5 mA/cm^2, pH_0 = 7.5

As shown in Figure *17*, when IBU was degraded by PMS alone in ROC, only 2 % removal in 30 min was observed because PMS has limited oxidation ability (redox potential E_0= 1.82 V) at room temperature and neutral pH (Bu et al., 2017; Qiong et al., 2021). Electrolysis using iron electrode (which can also be considered as electrocoagulation) achieved 18 % IBU removal in 30 minutes, it can be inferred that the coagulation mechanism contributed to IBU removal. Surprisingly, electrochemically activated peroxymonosulfate using iron as anode and graphite as the cathode (EC/PMS process) achieved complete removal in 30 minutes. In EC/PMS process, ferrous was generated electrochemically from the sacrificial iron anode (Eq. 1), which is responsible for PMS activation and leads to sulfate radical ($SO_4^{\bullet-}$) production (Eq. 2) (Qiong et al., 2021; Y. R. Wang & Chu, 2011). Sulfate radical attacks the IBU compound and quicken the IBU removal (Eq. 3). Besides this, PMS is also activated by electron gain and produce sulfate

radical (Eq. 4) and hydroxyl radical (Eq. 5) that further supports IBU oxidation (N. Yang et al., 2015). PMS gets activated through Fe^{3+} as well (Eq. 6) and produce peroxymonosulfate radical which is weaker than sulfate radical. In addition to that, chloride present in ROC reacts with PMS which leads to HOCl formation, which also attacked the IBU (Eq. 7) (Govindan et al., 2014; Y. R. Wang & Chu, 2011). Furthermore, there is possibility of Fe^{2+} regeneration on graphite cathode (Eq. 8) and this might enhance the IBU removal (Qiong et al., 2021). To verify the contribution of cathode and also the logic that iron anode is merely used to supply Fe^{2+} or direct oxidation occurred at the anode surface, PMS activation process was carried out using ferrous sulfate heptahydrate. According to Faraday's law ($C = (I*t)/(F*Z*V)$), for 30 min reaction with 2.5 mA/cm^2 current density (190 mA current) gives 99.12 mg Fe^{2+}. 99.12 mg Fe^{2+} was added in two ways, (i) total 99.12 mg Fe^{2+} was added at initial time point t=0, and (ii) 16.52 mg Fe^{2+} was added at t=0 and then 16.52 mg Fe^{2+} was added stepwise at every 5 minutes (t = 5, 10, 15, 20, 25 min) so that total 99.12 (16.52*6) mg Fe^{2+} was added in total 30 min. It is interesting to note that when total ferrous was added at start, removal was faster in first five minutes, but after that removal was slowed down and 46% removal was achieved in 30 min; whereas, when ferrous was added stepwise, it showed consistent removal throughout and 90% removal was achieved in 30 min (Figure 17). It implies that excess of ferrous at initial point quicken the removal in first five minutes because of more sulfate radical formation than EC/PMS process, but relatively high concentration of ferrous quenched sulfate radicals and slowed down the removal (Bu et al., 2017; Du, Zhang, et al., 2019). On the other hand, stepwise addition gave similar performance to that of EC/PMS process because in EC/PMS also Fe^{2+} generation is gradual; the only difference is, in former process Fe^{2+} was added manually and in later process it was generated electrochemically (Figure 17 & Figure 18). Though 10% more IBU removal in case of EC/PMS process could be attributed to Fe^{2+} regeneration from Fe^{3+} on cathode. As illustrated in Figure 17, EC/PMS and PMS activation by ferrous sulfate followed pseudo first order reaction kinetics. The apparent removal rate constants follow the order of EC/PMS (0.073 min^{-1}) > Fe^{2+} stepwise addition/PMS (0.071 min^{-1}) > Fe^{2+}/PMS (0.021 min^{-1}) > EC (0.0065 min^{-1}) > PMS (0.0008 min^{-1}).

$$Fe \rightarrow Fe^{2+} + 2e^{-} \text{ (Ferrous produced from anode)} \quad (6)$$

$$Fe^{2+} + HSO_5^{-} \rightarrow Fe^{3+} + SO_4^{\bullet-} + OH^{-} \text{ (PMS activation by } Fe^{2+}) \quad (7)$$

$SO_4^{\bullet-}$ + IBU → Intermediates → CO_2 + H_2O + SO_4^{2-} (IBU oxidation) (8)

HSO_5^- + e^- → $SO_4^{\bullet-}$ + OH^- (Electro activation of PMS) (9)

HSO_5^- + e^- → SO_4^{2-} + $^{\bullet}OH$ (Hydroxyl radical formation) (10)

Fe^{3+} + HSO_5^- → Fe^{2+} + $SO_5^{\bullet-}$ + H^+ (Peroxymonosulfate radical formation) (11)

Cl^- + HSO_5^- → SO_4^{2-} + HOCl (Reaction of PMS with Cl^- present in ROC) (12)

Fe^{3+} + e^- → Fe^{2+} (Fe^{2+} regeneration on cathode) (13)

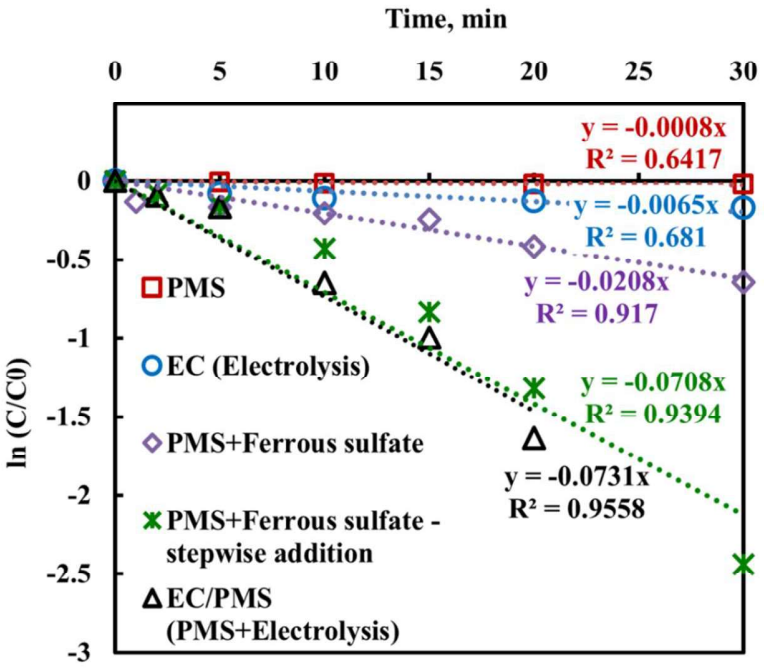

Figure 18: Comparison of different systems on the basis of reaction rate. Experimental conditions: $[IBU]_0$ = 10 mg/L, $[PMS]_0$ = 500 mg/L, $[Fe^{2+}]$ = 99 mg/L, current density = 2.5 mA/cm², pH_0 = 7.5

4.8 Contribution of reactive radical species in IBU removal using EC/PMS

As discussed in previous section, two principal contributors for IBU removal in EC/PMS process are sulfate radical and hydroxyl radical. To confirm the contribution of these radicals, quenching experiments were carried out in the presence of ethanol and tert butyl alcohol (TBA).

Ethanol quenches both sulfate radicals and hydroxyl radicals rapidly ($k_{sulfate\ radical} \sim 10^7\ M^{-1}s^{-1}$, $k_{hydroxyl\ radical} \sim 10^9\ M^{-1}s^{-1}$) because of two alpha hydrogen in ethanol whereas TBA largely quenches hydroxyl radicals ($k_{sulfate\ radical} \sim 10^5\ M^{-1}s^{-1}$, $k_{hydroxyl\ radical} \sim 10^8\ M^{-1}s^{-1}$) due to lack of alpha hydrogen (Qiong et al., 2021). Figure 19 indicates the change in IBU removal rate in presence of ethanol and TBA. The first order reaction rate constant remarkably decreased by 40% (0.0731 min^{-1} to 0.0436 min^{-1}) in presence of 32 mM ethanol and 61% (0.0731 min^{-1} to 0.0283 min^{-1}) in presence of 64 mM ethanol. On the other hand, drop in rate constant was not noteworthy in presence of TBA, which was 9% (0.0731 min^{-1} to 0.0665 min^{-1}) with 32 mM TBA and 18% (0.0731 min^{-1} to 0.0599 min^{-1}) with 64 mM TBA. IBU removal was less hindered by TBA and more by ethanol in ROC at neutral pH, which indicates that contribution of sulfate radical is higher than that of hydroxyl radical in EC/PMS process.

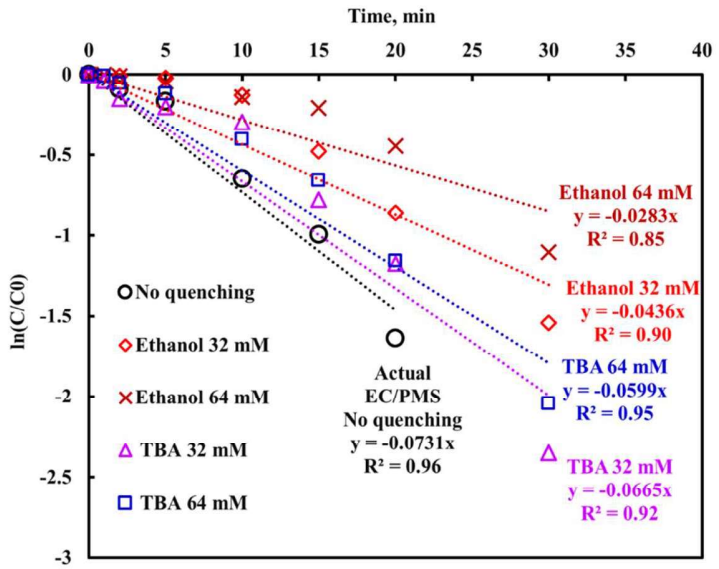

Figure 19: Effect of radical quenchers on IBU degradation. Experimental conditions: ROC, $[IBU]_0$ = 10 mg/L (0.05 mM), $[PMS]_0$ = 500 mg/L, current density = 2.5 mA/cm^2, pH_0 = 7.5

4.9 Results of response surface methodology

BBD model and analysis of variance (ANOVA): The PMS concentration and current density (which is in direct proportion with Fe^{2+} generation) apparently govern the EC/PMS process, as discussed in above sections. To confirm the effect of initial pH, single-factor experiments were carried out and it was found that pH also has significant role in EC/PMS process

for IBU removal. Therefore, the three level three factor Box–Behnken design (BBD) was performed to process the effect of individual factors and their interactions. The experimental results of IBU removal using EC/PMS for 30 min were obtained from run of 17 experimental sets. Results are tabulated for two responses i) % removal in 30 minutes, and ii) removal rate constant in min^{-1}(as long as process followed pseudo first order) as given in Table 6.

Table 6: Experimental design and conditions for RSM study of EC/PMS process

Run	Factor 1 A pH pH	Factor 2 B $[PMS]_0$ mg/L	Factor 3 C Current density mA/cm^2	Response 1 % Removal in 30 min %	Response 2 k min^{-1}
1	5.5	100	2.5	88.4	0.2275
2	5.5	500	0.525	64.5	0.0313
3	5.5	500	4.475	96.5	0.1807
4	5.5	900	2.5	90.8	0.0681
5	7.5	100	0.525	63.8	0.0369
6	7.5	100	4.475	63.6	0.2013
7	7.5	500	2.5	100	0.0777
8	7.5	500	2.5	100	0.0779
9	7.5	500	2.5	99	0.0800
10	7.5	500	2.5	99	0.0850
11	7.5	500	2.5	99	0.0848
12	7.5	900	0.525	18	0.0108
13	7.5	900	4.475	99.6	0.0654
14	9.5	100	2.5	23.1	0.0138
15	9.5	500	0.525	33.8	0.0147
16	9.5	500	4.475	95.9	0.1224
17	9.5	900	2.5	82.2	0.0487

The statistical analysis was carried out for both the responses. In case of Response 1 - % removal in 30 min, even with R^2=0.93 for Quadratic model, predicted R^2 was negative suggesting that model cannot be used for predictions. In case of Response 2 – removal rate constant, the Fit summary obtained from Design Expert 11 suggested that 2FI model fitted the experimental data well with R^2=0.93, Adjusted R^2=0.90, and Predicted R^2=0.77. The 2FI model includes sequential sum of squares for the interaction between two independent variables (i.e. AB, BC, and AC) along with individual variables. Except the interaction between current density and pH (coded term AC), all terms were significant with p values less than 0.05. The 2FI equation for removal rate constant

in terms of the three independent variables and two interactions with fit statistics is shown in Table 7. The 2FI equation showed that IBU removal rate constants increased at acidic pH with lesser PMS concentration and higher current densities, also interaction of pH and PMS contributed positively whereas interaction of PMS and current density negatively contributed in removal rate constant.

Table 7: 2FI Model and its Fit statistics from RSM study

k	**=**	**R^2:**	**0.93**
0.38087		Adjusted R^2:	0.90
-0.049609	****pH***	Predicted R^2:	0.77
-0.000458	****PMS***	Adeq Precision:	17.98
+0.047506	**** current density***	Std. Dev.:	0.0207
+0.000061	****pH * PMS***	Mean:	0.0828
-0.000035	****PMS * current density***	C.V. %:	24.97

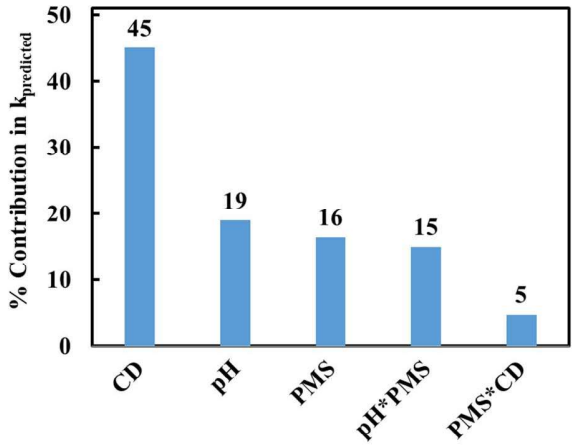

Figure 20: Pareto chart of the effect of current density, pH, PMS, and interactions of pH*PMS and PMS*current density

The Pareto chart shown in Figure 20 indicates the significance and contribution of all studied variables and their interactions in predicting the IBU removal rate constant. The current density is found to be the most significant variable, followed by pH, PMS Concertation, pH-PMS interaction, and PMS-current density interaction. Current density alone contributes the 45% in removal which indicates that Fe^{2+} generation is the rate limiting step in EC/PMS process.

The validity of using the 2FI model was ensured by analysis of variance (ANOVA), and the ANOVA results are abridged in Table 8. The F value was 29.42 and the corresponding p value

was less than 0.0001 indicative of high statistical significance and there was less than 0.01% chance that these values are due to noise (Rodriguez-Narvaez et al., 2020). Meanwhile, the lack-of-fit term was significant (p value < 0.05), which indicated that lack of fit error was more than pure error from replicated design points and the variation in response for these replicated points cannot be completely explained by 2FI model (Centre point was replicated five times).

Table 8: Analysis of variance (ANOVA) results for reduced 2FI model

Source	Sum of Squares	df	Mean Square	F-value	p-value	
Model	***0.0629***	***5***	***0.0126***	***29.42***	***< 0.0001***	***significant***
A-pH	0.0119	1	0.0119	27.73	0.0003	significant
B-PMS	0.0103	1	0.0103	24	0.0005	significant
C- current density	0.0283	1	0.0283	66.27	< 0.0001	significant
AB-pH*PMS	0.0094	1	0.0094	22.07	0.0007	significant
BC-PMS* current density	0.003	1	0.003	7.05	0.0224	significant
Residual	0.0047	11	0.0004			
Lack of Fit	0.0044	7	0.0006	8.55	0.0278	significant
Pure Error	0.0003	4	0.0001			
Cor Total	0.0676	16				

A reasonably well linear correlation between the predicted data from 2FI model and experimental removal rate constant data can be observed from Figure 21.

3D response surfaces and contour plots: Figure 22, Figure 23, and Figure 24 show the 3D response surfaces and their matching contour plots of IBU removal rate constants over PMS conc. and current density, pH and current density, and pH and PMS conc. respectively based on developed 2FI model. Figure 22 shows the effect of pH for given PMS conc. and current density on IBU removal rate constant. It can be observed that the acidic pH 5.5 is the most favourable for EC/PMS process with 100 mg/L PMS and 4.475 mA/cm^2 current density, where removal rate constant increased beyond 0.275 min^{-1}. As pH increased to 7.5, removal rate decreased to 0.2 min^{-1} for the same values of PMS and current density whereas alkaline pH 9.5 is not at all suitable for the EC/PMS process because removal rate constant dropped below 0.125 min^{-1}. As shown in Figure 22a, for pH 5.5, removal rate constant decreased with increasing PMS conc. and decreasing current density.

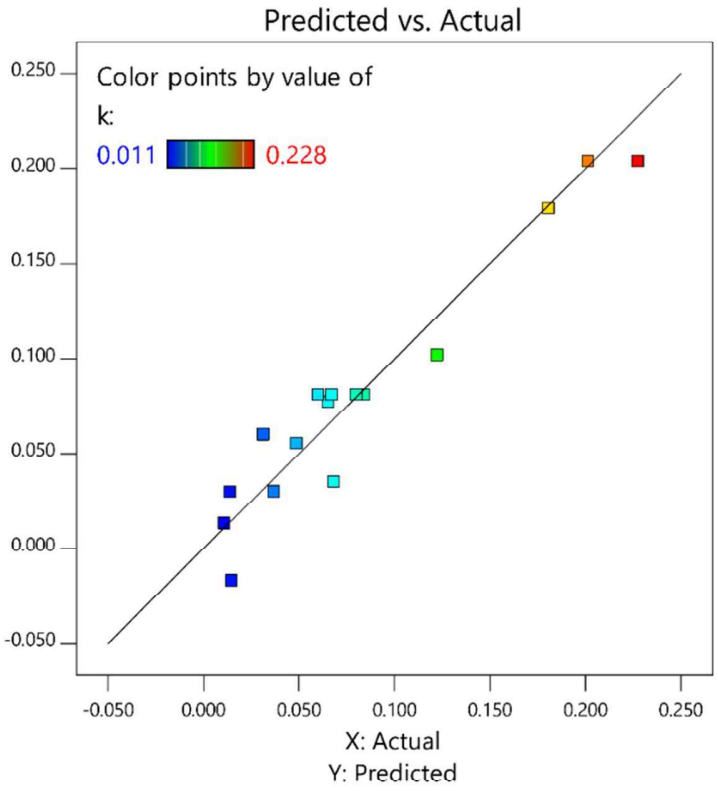

Figure 21: Predicted versus actual IBU removal rate constants

The availability of Fe^{2+} for PMS activation is highly dependent on pH. In alkaline pH, ferrous or ferric ions get converted to iron hydroxides and it leads to decrease in Fe^{2+} availability and the reduction of radical generation and ultimately slowing down the IBU removal. Figure 23 shows the effect of PMS concentration for given values of pH and current density. It is interesting to note that lower PMS conc. 100 mg/L is optimum for maximum IBU removal rate constant and rate constant decreased with increasing PMS concentration for similar combinations of pH and current density. For $[PMS]_0$=100 mg/L, as shown in Figure 23a, removal rate constant decreased with increase in pH and decreased current density. The reason behind this could probably be quenching of sulfate radical and hydroxyl radical by excess PMS at the start of PMS activation (Qiong et al., 2021). Figure 24 shows the effect of current density for given values of pH and PMS conc. It is quite obvious that increase in current density enhances the IBU removal, as the Fe^{2+} generation increases which activates the PMS. For initial pH=5.5 and PMS=100 mg/L, removal rate constant is highest - above 0.275 min^{-1} for higher current density 4.475 mA/cm^2. As current density decreased to 2.5 mA/cm^2, removal rate constant decreased to 0.2 min^{-1}; and further decrease in current density to 0.525 mA/cm^2 resulted in dropping of removal rate constant below

0.125 min^{-1}. It can be concluded from Figure 22, Figure 23, and Figure 24 that acidic pH, lowest initial PMS conc., and highest current density were promoting the rate constants for IBU removal using EC/PMS process.

Nonetheless it is important to note that higher removal rate does not necessarily lead to complete removal. Appendices F, G, and H showed the time course profiles for all 17 experimental sets clustered on the basis of pH, $[PMS]_0$, and current density respectively. As per Appendix F, only two combinations showed complete IBU removal in 30 min at initial pH=7.5 – i. $[PMS]_0$=500 mg/L and current density =2.5 mA/cm^2, and ii. $[PMS]_0$=900 mg/L and current density =4.475 mA/cm^2. In both these cases, $[PMS]_0$ to current density ratio was 200 and if converted to moles, PMS consumption to Fe^{2+} generation molar ratio was ~1.9 (for 30 min reaction time), which means one mole of Fe^{2+} reacted with almost two moles of PMS for maximum radical generation and both sulfate and hydroxyl radicals are generated as per the reaction shown in Eq. 9 (Sun et al., 2020).

$$2HSO_5^- + Fe^{2+} \rightarrow Fe^{3+} + SO_4^{\bullet-} + SO_4^{2-} + {}^{\bullet}OH + OH^- \quad (14)$$

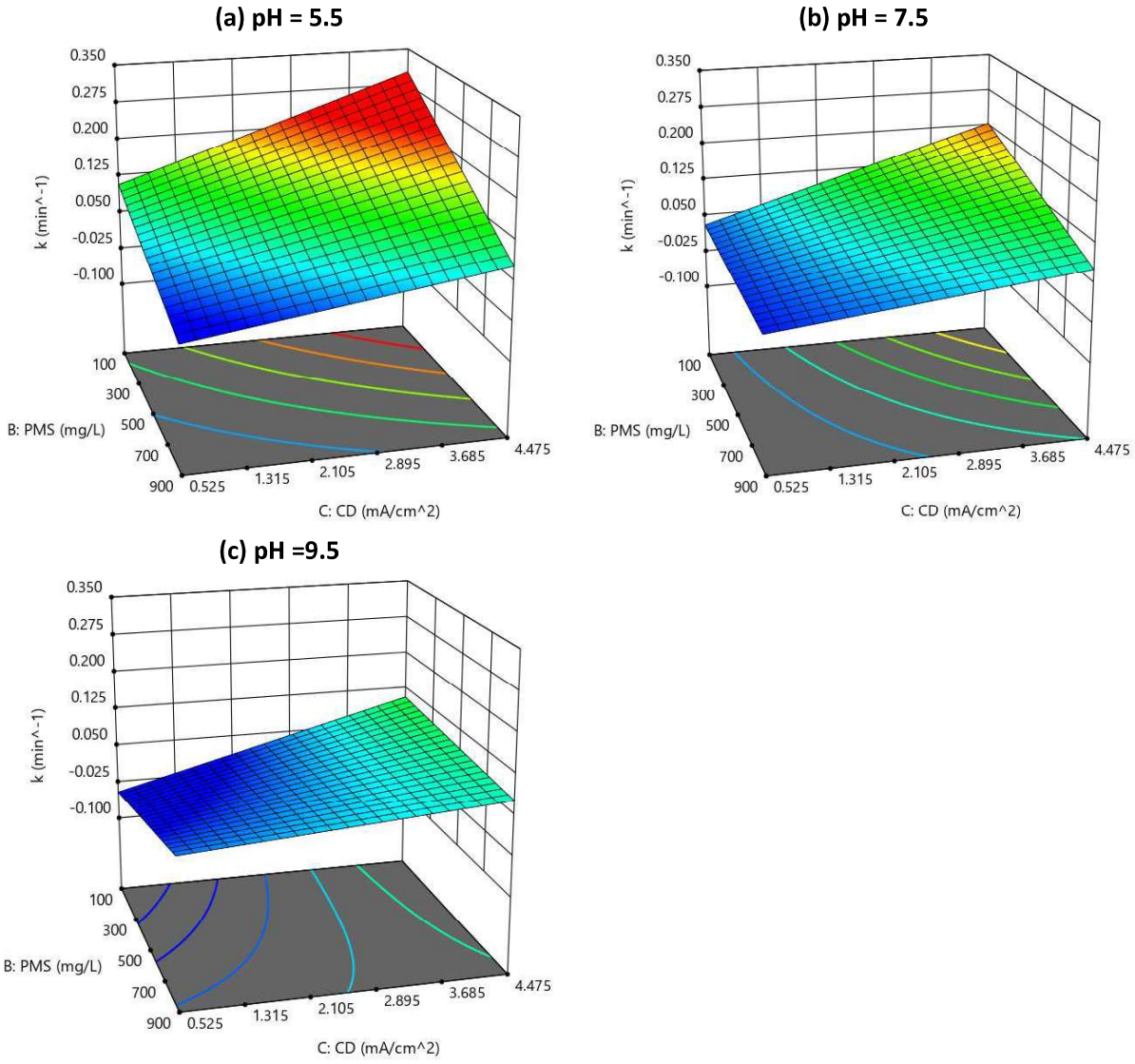

Figure 22: Effect of pH on IBU removal rate constant for various combinations of current densities and $[PMS]_0$. Experimental conditions: ROC, $[IBU]_0$ = 10 mg/L.

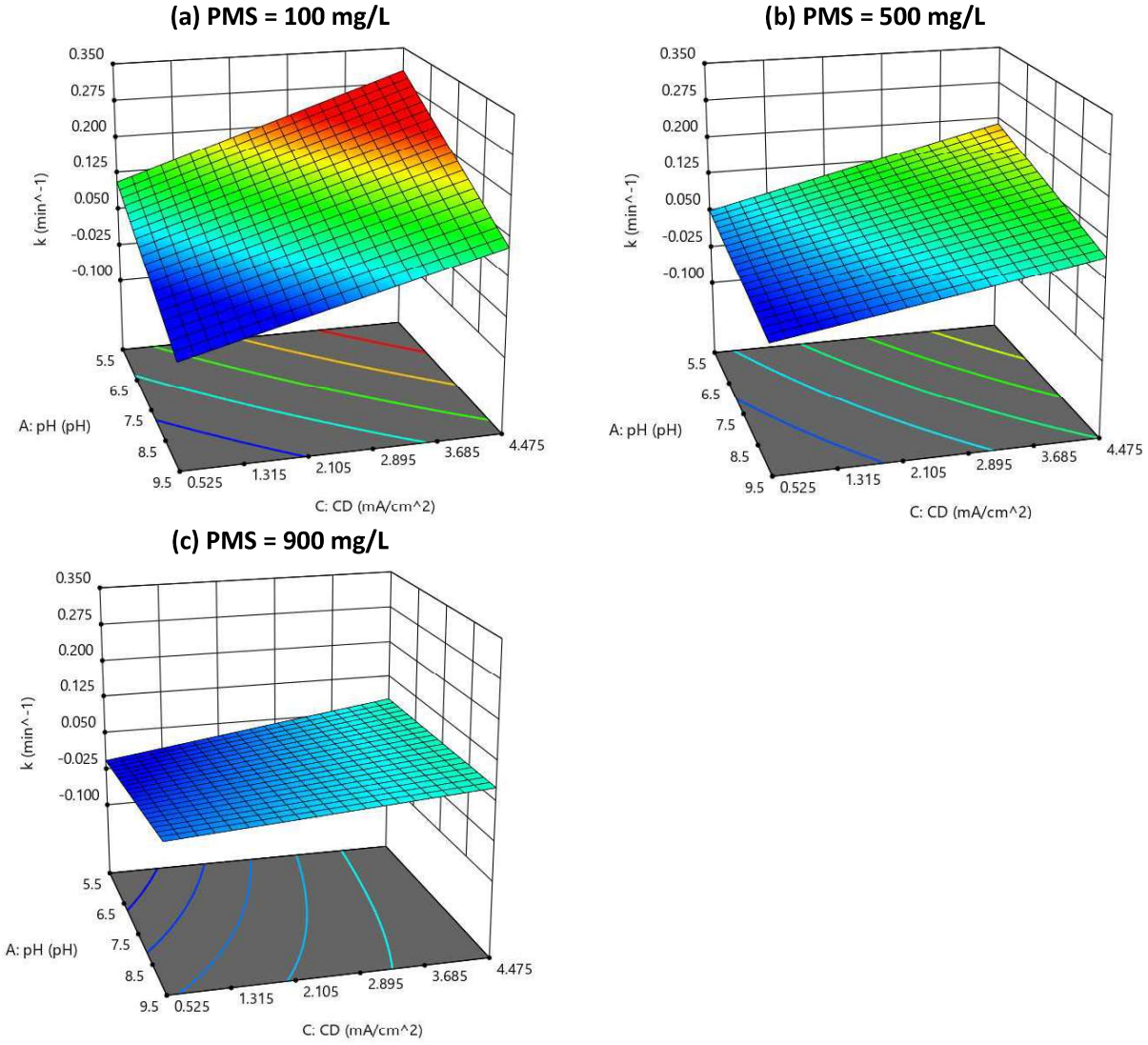

Figure 23: Effect of initial PMS concentration on IBU removal rate constant for various combinations of pH and current densities. Experimental conditions: ROC, $[IBU]_0$ = 10 mg/L.

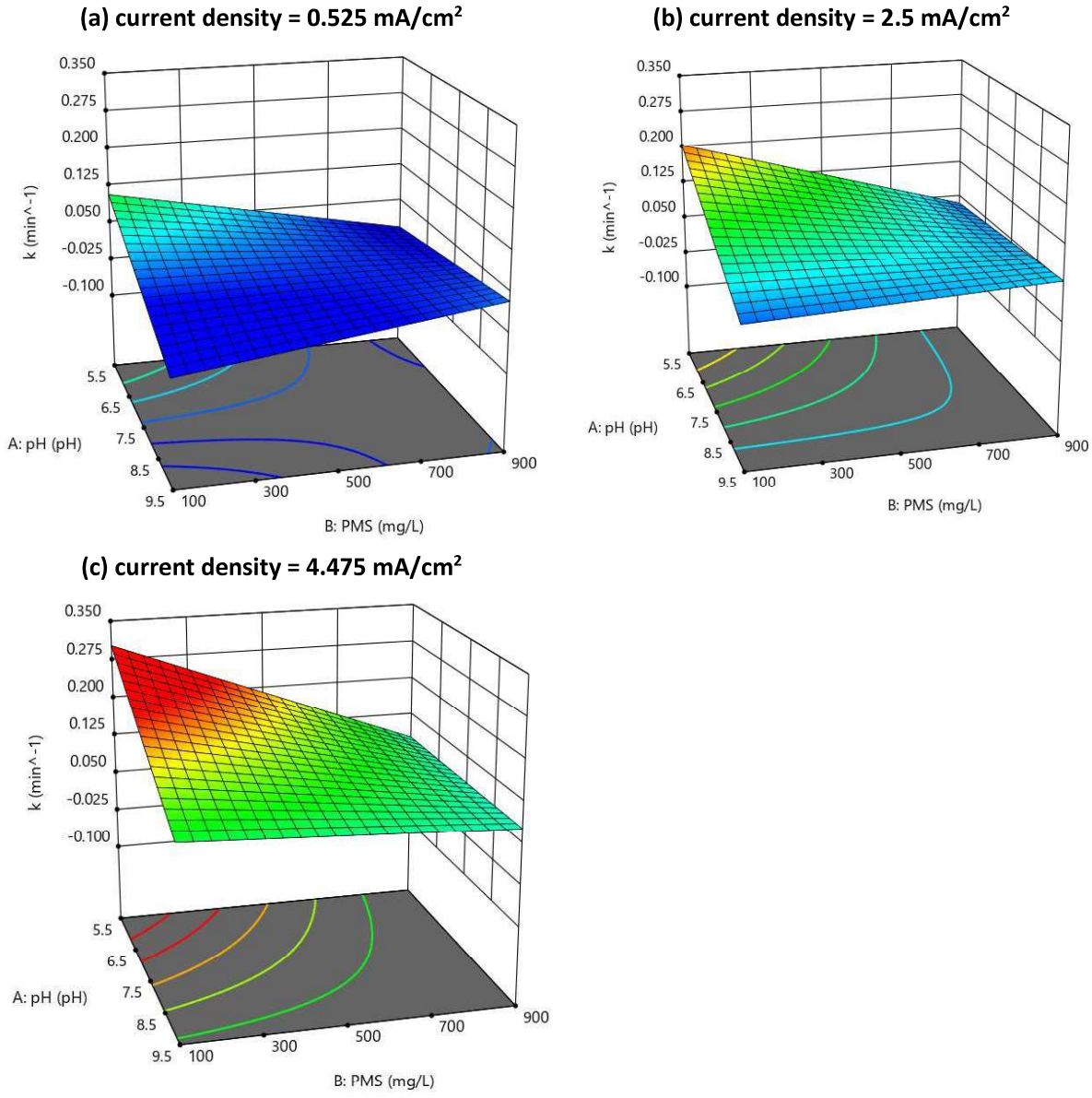

Figure 24: Effect of current density on IBU removal rate constant for various combinations of pH and $[PMS]_0$. Experimental conditions: ROC, $[IBU]_0$ = 10 mg/L.

If we carefully observe in Appendix F, it can be seen that there is no individual effect of pH on % IBU removal at the end of 30 min. More than 95% removal was achieved for all three pH for different combinations of $[PMS]_0$ and current density: for pH 5.5 and pH 9.5 - $[PMS]_0$=500 mg/L and current density =4.475 mA/cm^2; for pH 7.5 - $[PMS]_0$=500 mg/L and current density =2.5 mA/cm^2, $[PMS]_0$=900 mg/L and current density =4.475 mA/cm^2. Yet it is noticeable that % IBU removal is more than 60% in all cases for acidic pH 5.5 and ≥ 99% in two cases for pH 7.5. Similarly, it can be observed from Appendix G, that $[PMS]_0$ alone did not affect the % removal achieved 30 min but it is evident that maximum cases achieved more than 95% removal in case of 500 mg/L initial PMS conc. Also, in comparison with 0.525 mA/cm^2 current density other current density 2.5 and 4.475 mA/cm^2 performed much better in terms of % IBU removal in 30 min as shown in Appendix H. Hence, 3D plot was prepared for near neutral pH 7.5 to determine the combined effect of current density and $[PMS]_0$ on % IBU removal in 30 min. It is evident from Appendix I, that 500 mg/L $[PMS]_0$ and 2.5 mA/cm^2 current density are optimum for complete IBU removal at 7.5 pH and further increase in $[PMS]_0$ and current density did not contribute to faster removal but radicals generated with the excess PMS and Fe^{2+} would be quenched by themselves.

It is fascinating to observe the effect of $[PMS]_0$ to current density ratio on % IBU removal and removal rate constants as depicted in Appendix J. It is evident that high $[PMS]_0$ to current density ratio neither favouring % IBU removal nor removal rate constant. Lower ratios initially supported the removal rate constant for all pH (there is only one exception for alkaline pH 9.5, reason could be the lowest $[PMS]_0$) and removal rate constant started decreasing as $[PMS]_0$ to current density ratio increased. Whereas, for % IBU removal in 30 min, 200 was found to be the optimum ratio for all pH and %removal was > 95% i.e. 96.5%, 100%, and 95.9% for 5.5, 7.5, and 9.5 pH respectively.

4.10 Performance in continuous flow mode

As discussed in previous section, 7.5 initial pH, 500 mg/L $[PMS]_0$, and 2.5 mA/cm^2 achieved complete IBU removal using EC/PMS process. Thus, this combination was selected for continuous flow experiments. Reactor was initially operated in batch mode for 30 minutes and then fresh solution containing 10 mg/L IBU and 500 mg/L $[PMS]_0$ was introduced in the reactor. The flow was kept 2 L/h for the preliminary experiment and samples were withdrawn after 15

minutes from the switch to continuous mode. As shown in Figure 25a, IBU conc. in the outlet of continuous flow reactor was ranging from 0.2 to 0.5 mg/L (average 0.35 mg/L, 96.8% removal) and average values of Fe^{2+}, Fe^{3+}, and total Fe conc. were 9.9, 37.6, and 47.5 mg/L respectively. It is noteworthy that while in batch mode (-30 to 0 min), 500 mg/L PMS was added at the start and from that point to next 30 min, PMS was consumed and Fe^{2+} and Fe^{3+} was generated continuously. As the feed started, PMS was introduced again with IBU and Fe^{2+} was further consumed in PMS activation which leaded to decrease in Fe^{2+} conc. and also Fe^{3+} conc. The molar ratio of IBU: Fe^{2+}: PMS was 1: 37.5: 68.5, for 2 L/h flow and 30 min residence time. To achieve the complete IBU removal and maximum consumption of Fe^{2+} in PMS activation (maximum current efficiency), flow rates were increased to 2.5, 3, and 4 L/h giving residence time (RT) 24, 20, and 15 min respectively (Kobya et al., 2016; Sravanth et al., 2020). As illustrated in Figure 25b, c, and d, increased flow attained more % IBU removal and lesser residual Fe^{2+} appeared in outlet. For 2.5, 3, and 4 L/h flow, IBU: Fe^{2+}: PMS molar ratios were 1: 30: 68.5, 1: 25: 68.5, and 1: 19: 68 respectively and average % IBU removal were 97.8%, 98.7%, and 99.5% respectively. Here also, there is strong correlation between PMS to Fe^{2+} ratio and % IBU removal. As PMS to Fe^{2+} ratio increased from 1.8 to 3.6, average % IBU removal increased from 96.5% to 99.5%.

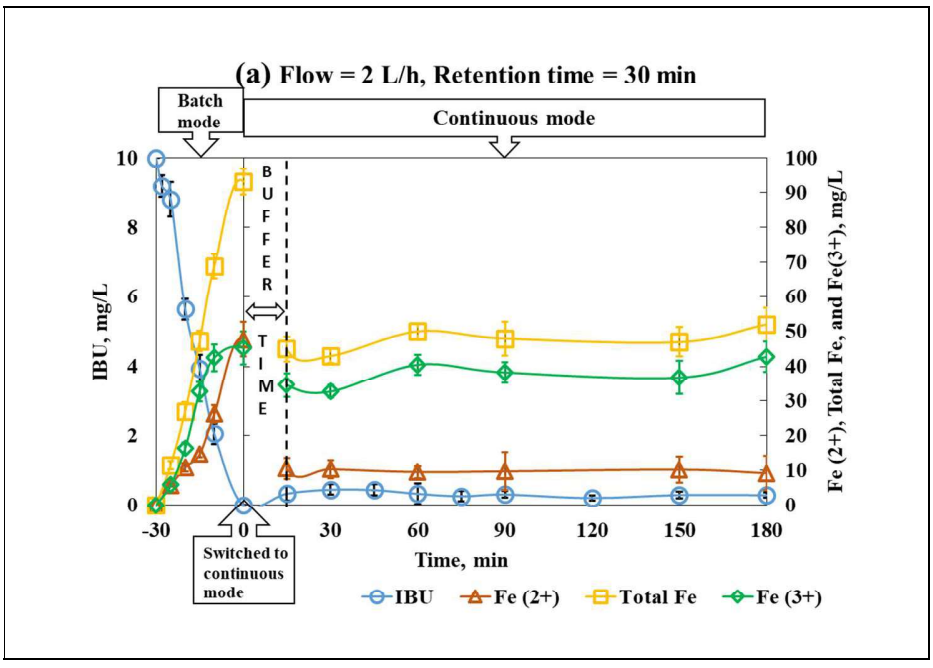

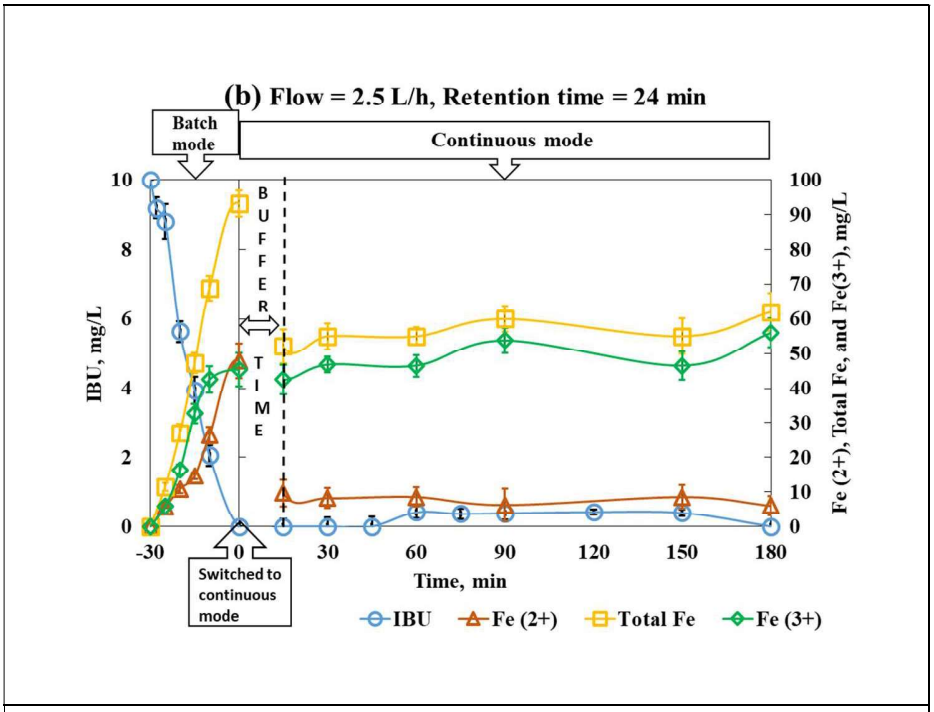
(b) Flow = 2.5 L/h, Retention time = 24 min
Batch mode
Continuous mode
BUFFER TIME
IBU, mg/L
Fe (2+), Total Fe, and Fe(3+), mg/L
Switched to continuous mode
Time, min
IBU
Fe (2+)
Total Fe
Fe (3+)

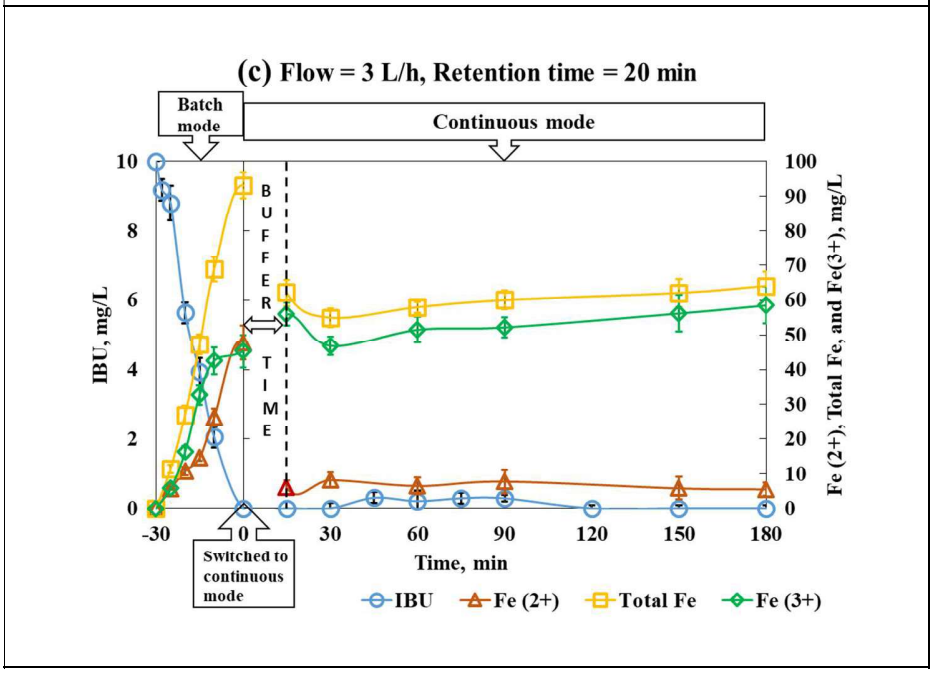
(c) Flow = 3 L/h, Retention time = 20 min
Batch mode
Continuous mode
BUFFER TIME
IBU, mg/L
Fe (2+), Total Fe, and Fe(3+), mg/L
Switched to continuous mode
Time, min
IBU
Fe (2+)
Total Fe
Fe (3+)

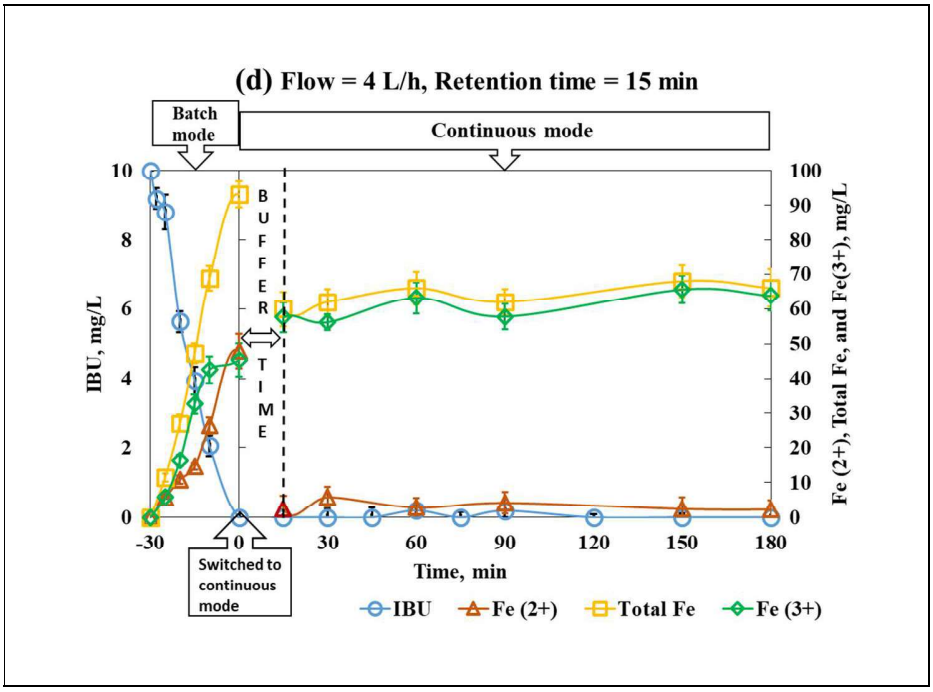

Figure 25: Effect of flow (residence time - RT) on the performance of continuous EC/PMS process (a) Flow = 2 L/h, RT = 30 min, (b) Flow = 2.5 L/h, RT = 24 min, (c) Flow = 3 L/h, RT = 20 min, (d) Flow = 4 L/h, RT = 15 min.

4.11 Results of LC-MS analysis

LC-MS analysis was carried out to identify the intermediates formed while EO of DCF and EC/PMS of IBU in ROC. As depicted in Figure 8 and Figure 9, during EO of DCF, two intermediates were formed at RT 8.5 min and 9.1 min. To identify the molecular mass and structure of these compounds, LC-MS analysis was carried out. As shown in Figure 26, mass of DCF was confirmed as m/z 296. Mass of $IP_{8.5}$ was found to be m/z 310.2 and mass of $IP_{9.1}$ was found to be m/z 314.1. According to the fragmentation pattern and published reports, the hydroxylation products of DCF from indirect oxidation were proposed as shown in the Figure 26.

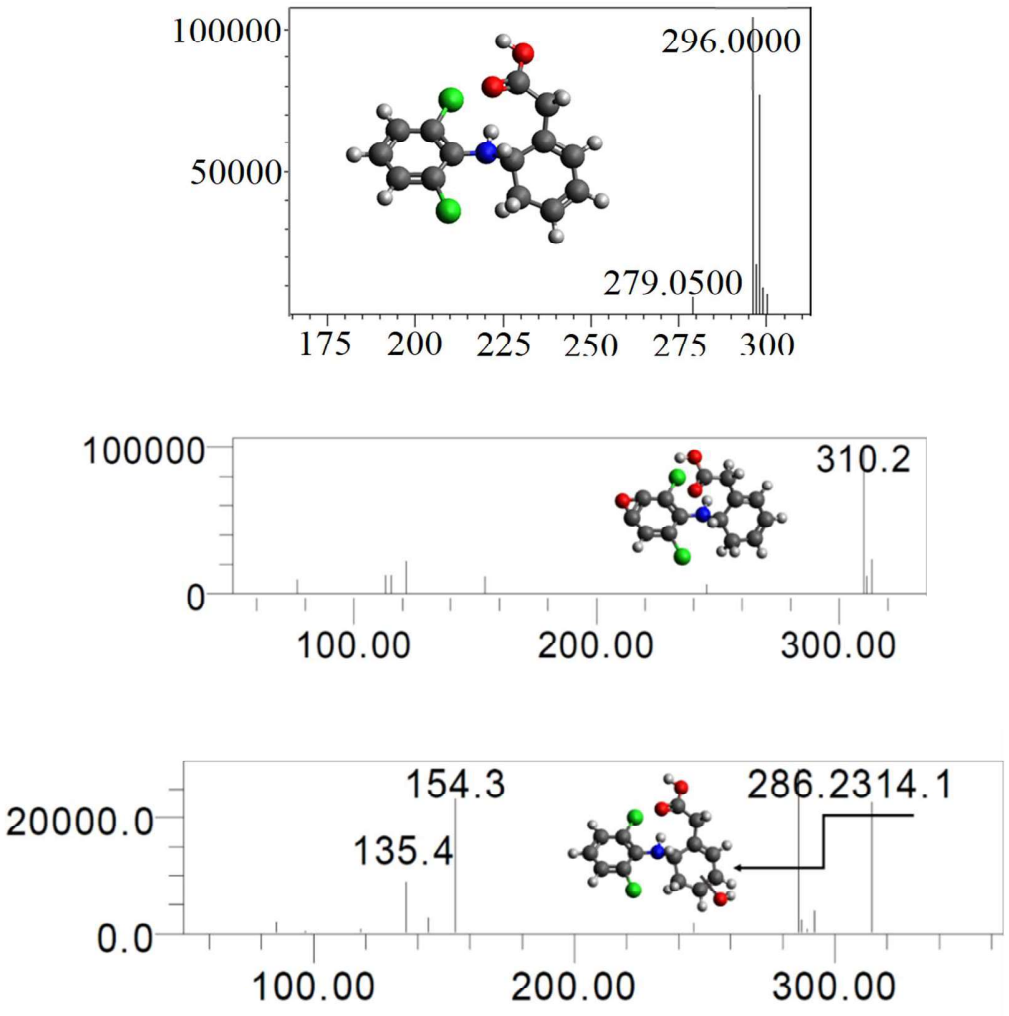

Figure 26: LC-MS spectrums of DCF (m/z 296), $IP_{8.5}$ (m/z 310), and $IP_{9.1}$ (m/z 314). (Colour coding: Black=Carbon, Grey=Hydrogen, Red=Oxygen, Green=Chlorine, Blue=Nitrogen).

Similarly, the intermediate was observed in HPLC chromatograms of samples containing IBU after EC/PMS process. IBU appeared at 222 nm and when sample was scanned at 260 nm, the intermediate was increasing with the decrease in IBU conc. Therefore, LC-MS analysis was carried out to identify the mass and structure of the intermediate appearing at 260 nm (refer Appendix K). As depicted in Figure 27, IBU was confirmed at 222 nm with m/z 206.3, and m/z of the intermediate was found to be 238. Quite similar to the EO of DCF, here also, hydroxylation product of IBU was proposed as suggested by published literature and fragmentation pattern. Brillas, 2022 and Y. Xiang et al., 2016 also reported this oxidation product of IBU using UV/chlorination and Catalytic Ozonation/PMS respectively. The reason could be the easy conversion of sulfate radical to hydroxyl radical in aqueous matrix (J. Li et al., 2022; T. Liu et al., 2023) as shown in Eq. 15.

$$SO_4^{\bullet-} + OH^- \rightarrow SO_4^{2-} + {}^{\bullet}OH \qquad (15)$$

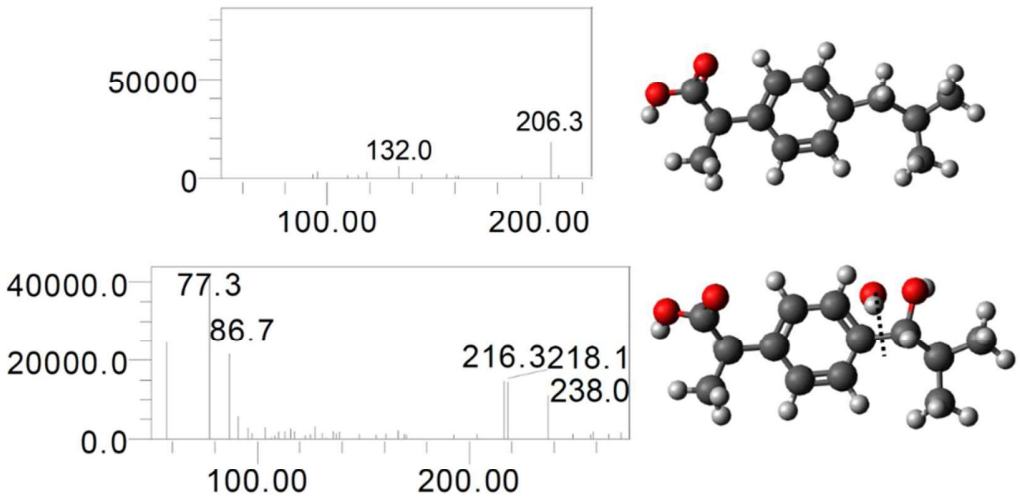

Figure 27: LC-MS spectrums of IBU (m/z 206.3) and IP$_{@\ 260\ nm}$ (m/z 238). (Colour coding: Black=Carbon, Grey=Hydrogen, Red=Oxygen, Green=Chlorine, Blue=Nitrogen).